Exact Analysis of Parallel Resonant DC-DC Converter using Phase Shift Modulation

Vishal Anand A G*, Anirban Pal†, Ranganathan Gurunathan*, Kaushik Basu†
*Bloom Energy (I) Pvt Ltd, Bangalore
{vanand,rgurunat}@bloomenergy.com
†Department of Electrical Engineering, Indian Institute of Science, Bangalore
{anirbanp,kbasu}@iisc.ac.in

2021 IEEE Energy Conversion Congress and Exposition (ECCE) | 978-1-7281-5135-9/21/$31.00 ©2021 IEEE | DOI: 10.1109/ECCE47101.2021.9595471

***Abstract*—In this paper, the exact analysis of the Parallel Resonant (PR) DC-DC converter using constant frequency phase shift modulation is presented. Variable frequency modulation for control of resonant converters has some challenges in implementation like EMI filter design, switch driver design etc.. Hence, fixed frequency Phase Shift Modulation (PSM) is preferred in control of parallel resonant DC-DC converter. However, the analysis of PR converter using PSM is carried out using Fundamental harmonic approximation that ignores harmonics and results in erroneous estimation. In order to improve the accuracy and to quantify the intermediate converter parameters, an exact analysis of the PR converter using fixed frequency PSM is discussed. The analysis is important in design and control of the converter. Expression for converter gain and other parameters of interest are derived. Accuracy of the analysis is verified through simulation and experiment of a $1.5kW$ prototype.**

***Index Terms*—Resonant Converter, State Plane Analysis, Variable Frequency Modulation, Zero voltage switching, Parallel resonance, Phase Shift modulation, Fundamental Harmonic Approximation**

I. Introduction

The isolated DC-DC converters today find their use in a variety of applications like Electric traction [1], grid integration of renewable energy sources [2], high voltage converters and other power supplies. Buck derived phase-shifted full bridge converters are simple to design and control due to fixed frequency operation. But this converter suffers from low light load efficiency and high voltage stress due to oscillations introduced by parasitic capacitances of the secondary diodes [3]. Resonance based power conversion overcome these problems in such applications and has gained lot of attention due to inherent benefits like wide soft switching range, low EMI etc. [4]–[6]. **S**eries **R**esonant (SR) [7] and **P**arallel **R**esonant (PR) [8] are popular two element topologies while LLC, LCC and LCL-T are more prevalent among three element converters. The control of resonant converters is implemented either using **V**ariable **F**requency **M**odulation (VFM) or at constant switching frequency using **P**hase **S**hift **M**odulation [9]. Control of the resonant converter under variable frequency modulation has some disadvantages like difficulties in design of magnetics and filters, increased power losses at higher frequency etc. [10]. Due to these reasons, a renewed focus to operate resonant converters under constant switching frequency to maximize the benefits from soft-switching is observed.

A number of applications rely on the benefits of resonant power conversion under constant switching frequency. Wireless power transfer [11], Inductive cap sealing [12] and unregulated front-end LLC converters [13] are some of these areas. In these applications, the converter is typically operating at or close to the resonant frequency as the circulating reactive current is minimum at this point. The understanding of the converter operation under this condition is critical to arrive at the optimum design of the resonant tank components.

The operation of resonant converters is piece-wise linear as different operating modes are observed within a switching cycle. In order to simplify the analysis and be able to use linear analysis techniques for resonant converters, a number of methods have been proposed in literature [14]. Majority of these methods rely on **F**undamental **H**armonic **A**pproximation (FHA) wherein the converter is analyzed only at the switching frequency and all other harmonics are ignored. Though this method provides the ease of analysis, it has been reported that there's significant error introduced due to this approximation [15]. State-plane based exact analysis has been reported to arrive at the exact values of converter gain and intermediate converter operating points [16]. Similarly, time domain based analytical techniques have also been reported for the series and LLC topologies [17]. However, the primary focus of the reported work in the area of exact analysis is using VFM.

In this paper, a detailed circuit analysis of PR converter which is controlled at constant switching frequency using Phase shift modulation. The commonly used PR structure followed by a LC filter is considered here. The major contributions are given below (a) Exact analysis of the converter operation is presented using state plane analysis (b) Step by step approach to arrive at the closed form expression of the converter gain. Additionally, closed form expressions for intermediate voltages and currents are derived. (c) A 1.0kW, 390V PR prototype is built and tested. The experimental results verify the theoretical analysis of mode by mode converter operation.

The organization of this paper is as follows. Detailed circuit operation using state plane analysis is presented in Section II. Closed form expression of output voltage and other component stresses of interest is given in section III. Experimental results verifying converter operation are given in section IV.

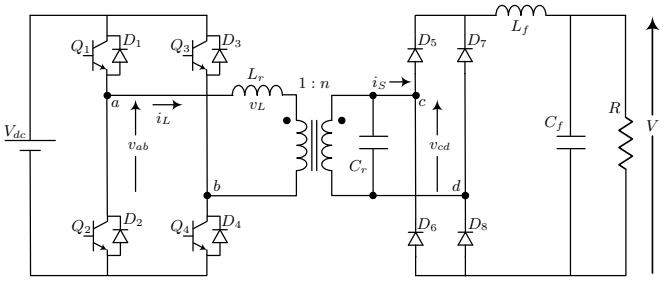

Fig. 1. Circuit topology of parallel resonant converter

II. Steady State Analysis

A **P**arallel **R**esonant (PR) based DC-DC converter is shown in Fig. 1. The exact analysis of the PR converter under **V**ariable **F**requency **M**odulation (VFM) is well understood [16]. Multiple operating modes of the converter are arrived at by idealizing the switching components and considering piece-wise linear circuits to carry out the analysis. State plane based technique is then used to arrive at the closed for expression form the converter gain. For the simplicity of the analysis, the relevant parameters are converted in per unit form. The base quantities are provided in Table I. Per unit quantities are shown in Table II. In order to simplify the analysis of the converter

TABLE I
PER-UNITISATION BASE PARAMETERS

Description	Formula
Base Voltage, V_b	nV_{dc}
Base Impedance, R_b	$n\sqrt{L_r/C_r}$
Base Current, I_b	V_b/R_b
Base Frequency, f_b	$1/2\pi n\sqrt{L_rC_r}$

the entire circuit can be reflected to the secondary side of the converter shown in Fig. 1. The output LC filter ensures that output voltage, V shall remain stable and ripple free. The operation of the secondary diode bridge can be represented

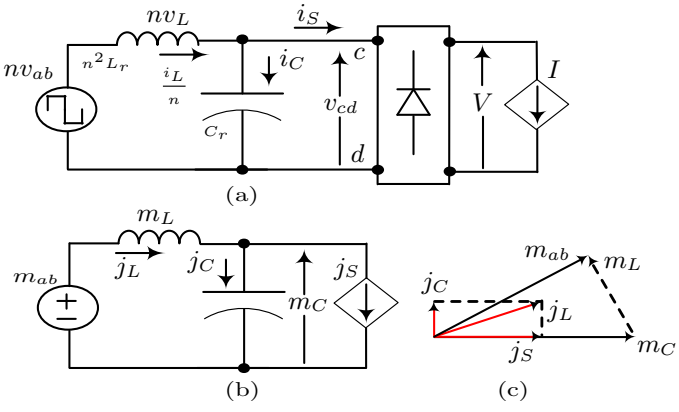

Fig. 2. Parallel Resonant structure of the HFL converter (a) Reduced circuit of the converter reflected onto the secondary side of transformer with the load modeled as a current sink (b) Per-unitized equivalent circuit and (c) Phasor analysis of the per-unitized equivalent circuit

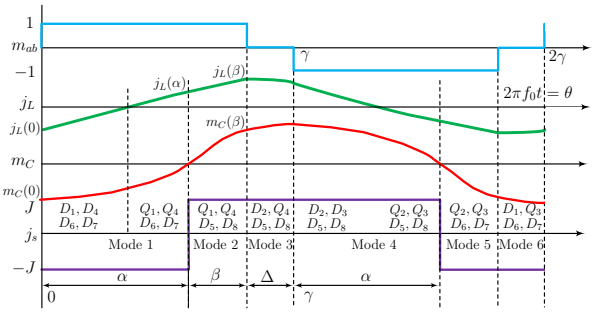

Fig. 3. Steady state waveforms of the PR converter in the PWM Mode of operation

TABLE II
PU QUANTITIES

Description	Formula
Resonant capacitor voltage, m_C	v_{cd}/V_b
Resonant inductor current, j_L	i_L/I_b
Switching frequency, F	f_s/f_b
Rectifier input current, j_S	i_S/I_b
Inductance voltage drop, m_L	v_L/V_b
Angular half-period, γ	π/F
Output current, J	I/I_b
Voltage gain, M	V/V_b
Angle variable, θ	$2\pi f_b t$
Tank Voltage, m_{ab}	v_{ab}/V_b

by a voltage dependent current source, I as shown in Fig. 2(a). This equivalent circuit can be further reduced to represent the converter in **P**er **U**nit (PU) model as shown in Fig. 2(b). Devices Q_1 to Q_4 in Fig. 1 are switched to generate the quasi square wave input, m_{ab}. Fig. 2(c) shows the approximated phasors considering the fundamental harmonic. Even though FHA is not used in the analysis here, it does provide an idea of the relative polarities of the waveforms of interest under steady state. When the switching frequency of the converter is greater than the resonant frequency, the parallel resonant tank provides an inductive impedance. From the phasor, it's clear that the fundamental component of m_{ab} shall lead the inductor current, j_L and capacitor voltage, m_C. The waveforms of interest in the operation of the converter are shown in Fig. 3. Applying phasor analysis shown in Fig. 2(c), it can be inferred that $m_C(0)$ and $j_L(0)$ are negative during the positive zero crossing of m_{ab} as can be seen in Fig. 3. Based on the devices in conduction, the operation of the PR converter in PWM can be distinguished into multiple modes as shown here. Due to the presence of half wave symmetry, Modes 4 to 6 are not discussed and can be inferred from operation in Modes 1 to 3.

A. *Mode 1:* $0 < \theta < \alpha$

This mode starts at instant, 0 in Fig. 3 when switch Q_2 is turned OFF. Since the direction of current i_L is negative, anti-parallel diode, D_1 conducts the current and ensures ZVS turn ON of device Q_1. After the current, j_L becomes positive, device Q_1 takes over the current conduction from diode,

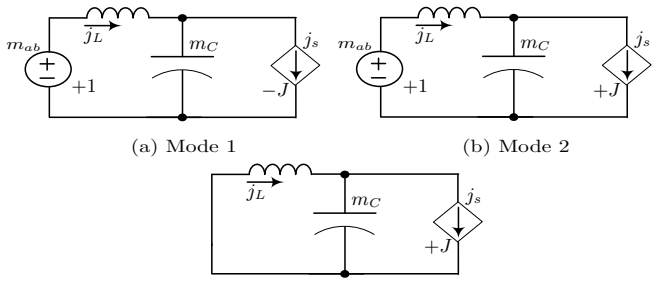

Fig. 4. Reduced equivalent circuit of the PR converter under different operating modes (a) Equivalent circuit in Mode 1 (b) Equivalent circuit in Mode 2 and (c) Equivalent circuit in Mode 3

D_1. The effective equivalent circuit of the converter during this mode of operation is shown in Fig. 4(a). The governing equations of the converter under this mode is given below

$$\frac{dj_L}{d\theta} + m_C = 1 \qquad (1) \qquad\qquad \frac{dm_C}{d\theta} - J = j_L \qquad (2)$$

Moreover, based on the phasor diagram shown in Fig. 2(c), it can be observed that the inductor current, j_L shall lead the capacitor voltage, m_C. This mode ends at α when the capacitor voltage, m_C becomes greater than 0.

B. Mode 2: $\alpha < \theta < \alpha + \beta$

This mode starts at instant, α in Fig. 3 when diodes D_5, D_8 take over the conduction from D_6 and D_7. Due to the diode commutation, the polarity of the current sink is reversed as shown in the effective equivalent circuit Fig. 4(b). The governing equations of the converter under this mode is given below

$$\frac{dj_L}{d\theta} + m_C = 1 \qquad (3) \qquad\qquad \frac{dm_C}{d\theta} + J = j_L \qquad (4)$$

This mode ends when device Q_1 is turned OFF at the instant $\alpha + \beta$.

C. Mode 3: $\alpha + \beta < \theta < \gamma$

This mode starts at instant, $\alpha + \beta$ in Fig. 3 when device Q_1 is turned OFF. The presence of device capacitance ensures **Z**ero **V**oltage **S**witching (ZVS) turn OFF of Q_1. The governing equations of the converter under this mode is given below

$$\frac{dj_L}{d\theta} + m_C = 0 \qquad (5) \qquad\qquad \frac{dm_C}{d\theta} + J = j_L \qquad (6)$$

This mode ends when device Q_4 is turned OFF at γ.

The operation of the converter in modes 4 to 6 is symmetric with Modes 1 to 3 and so is not discussed here. The evaluation of the converter gain as a function of the converter operational parameters like normalized switching frequency, F, load, J and duty ratio of operation, Δ is described below.

III. Converter Gain

The variation between inductor current, j_L and capacitor voltage, m_C shown in Fig 3 can be plotted with respect to each other to get the state plane portrait of the converter. This is shown in Fig. 5. The six operating modes described above are highlighted in Fig 5. As shown in Fig 3, average value of rectified capacitor voltage, $|m_C|$ is applied across the load. The converter gain is arrived at by getting a closed form expression for this voltage as given in (7). The expression for $m_C(\theta)$ is written from (1), (3) and (5). This is substituted in (7) to arrive at (8).

$$M = \frac{1}{\gamma}\int_{\alpha}^{\alpha+\gamma} m_C(\theta)d\theta \qquad (7)$$

$$M = \frac{1}{\gamma}\left\{\left\{\int_{\alpha}^{\alpha+\beta} 1d\theta + \int_{\gamma}^{\gamma+\alpha} -1d\theta\right\} - \left\{\int_{\alpha}^{\gamma+\alpha} 1.dm_C\right\}\right\} \qquad (8)$$

(8) can be further reduced to arrive at the expression below which equates M with angular half-period, γ which in turn is a function of the operating frequency, F and the intermediate load dependent current, $j_L(\alpha)$ as shown in Fig. 3.

$$\frac{M\pi}{2F} = \phi + j_L(\alpha) \qquad (9) \qquad\qquad \phi = \frac{\beta - \alpha}{2} \qquad (10)$$

The converter gain, M in the PWM mode can now be derived if the intermediate parameters, ϕ and $j_L(\alpha)$ can be found as function of the parameters of interest. The subsequent steps to arrive at the converter gain in the VFM mode of operation is described in [18]. However, the analysis for the PWM mode of operation is a bit more involved due to the presence of zero state. The following sections describe the steps to arrive at the closed form of the converter gain in this mode of operation. The state plane analysis technique uses basic trigonometric relationships to reduce the complexity of the equations.

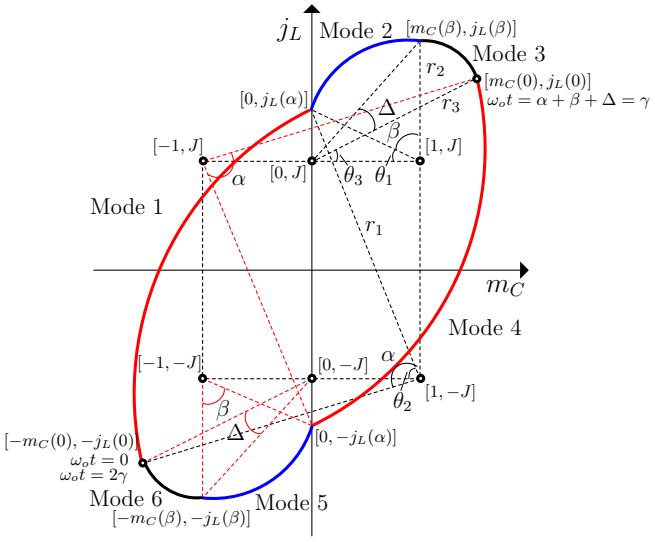

Fig. 5. State plane portrait of the PR converter in PWM Mode

A. Determination of arc radii

The arc radii of the different piece-wise circular arcs in Fig. 5 shall be eliminated using basic trigonometric relationships. Fig. 6 shows 3 piece-wise arcs at the boundaries between different modes of operation. Based on Fig. 6(a), the following

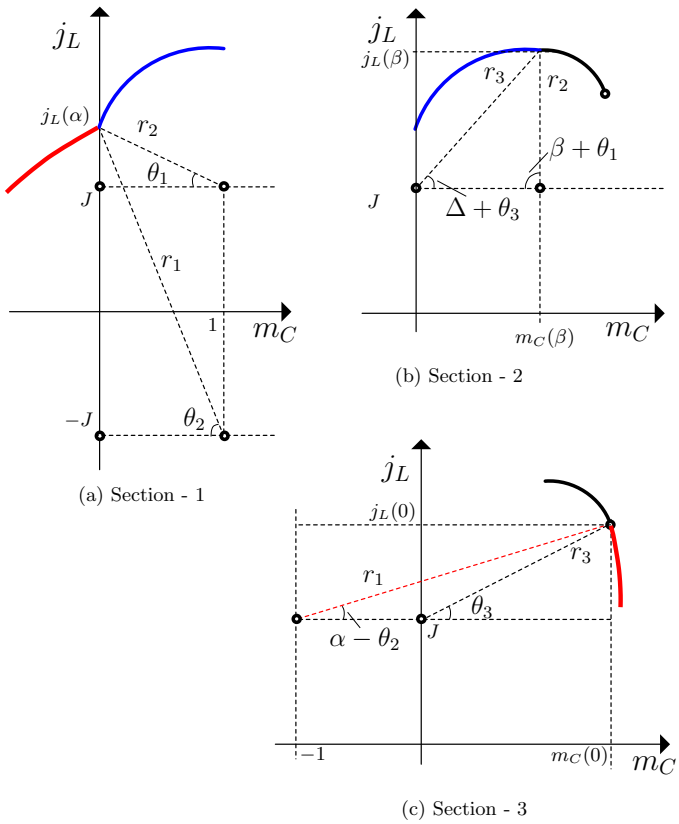

(a) Section - 1

(b) Section - 2

(c) Section - 3

Fig. 6. Section of the State Plane to determine arc radii

relationships can be arrived at that relates radii, r_1 and r_2.

$$r_2 \sin\theta_1 = j_L(\alpha) - J \quad (11) \qquad r_1 \sin\theta_2 = j_L(\alpha) + J \quad (13)$$

$$r_2 \cos\theta_1 = 1 \quad (12) \qquad r_1 \cos\theta_2 = 1 \quad (14)$$

Based on Fig. 6(b), the following relationships can be arrived at that relates radii, r_2 and r_3.

$$r_2 \sin(\beta+\theta_1) = j_L(\beta) - J \quad (15) \qquad r_3 \sin(\Delta+\theta_3) = j_L(\beta) - J \quad (17)$$

$$r_2 \cos(\beta+\theta_1) = 1 - m_C(\beta) \quad (16) \qquad r_3 \cos(\Delta+\theta_3) = m_C(\beta) \quad (18)$$

Based on Fig. 6(c), the following relationships can be arrived at that relates radii, r_3 and r_1.

$$r_1 \sin(\alpha-\theta_2) = j_L(0) - J \quad (19) \qquad r_3 \sin(\theta_3) = j_L(0) - J \quad (21)$$

$$r_1 \cos(\alpha-\theta_2) = m_C(0) + 1 \quad (20) \qquad r_3 \cos(\theta_3) = m_C(0) \quad (22)$$

Expanding (17) and substituting for internal trigonometric terms of r_3 from (21) and (22), we have the following relationship

$$m_C(0)\sin\Delta + [j_L(0) - J]\cos\Delta = j_L(\beta) - J \quad (23)$$

$$m_C(0)\cos\Delta - [j_L(0) - J]\sin\Delta = m_C(\beta) \quad (24)$$

Expanding (19) and substituting for internal trigonometric terms of r_1 from (13) and (14), we have the following relationship

$$\sin\alpha - [j_L(\alpha) + J]\cos\alpha = j_L(0) - J \quad (25)$$

$$[j(\alpha) + J]\sin\alpha + \cos\alpha = m_C(0) + 1 \quad (26)$$

Expanding (15) and substituting for internal trigonometric terms of r_2 from (11) and (12), we have the following relationship

$$\sin\beta + [j_L(\alpha) - J]\cos\beta = j_L(\beta) - J \quad (27)$$

$$-[j(\alpha) - J]\sin\beta + \cos\beta = 1 - m_C(\beta) \quad (28)$$

Equating (23), (27) and using the expression derived in (26) for $m_C(0)$ in (23), the following relationship can be arrived at by rearranging the terms and using basic algebra

$$\sin(\Delta+\alpha) - [j_L(\alpha) + J]\cos(\Delta+\alpha) = [j_L(\alpha) - J]\cos(\beta) + \sin\Delta + \sin\beta \quad (29)$$

The following relationship is defined as per the waveforms shown in Fig. 3.

$$\alpha + \beta + \Delta = \gamma \quad (30)$$

Substituting (30) and (10) in (29) and replacing γ with $\frac{\pi}{F}$, the following relationship can be derived by using basic trigonometric identities.

$$-\sin\left(\phi - \frac{\Delta}{2}\right)\left[\cos\frac{\pi}{2F} + J\sin\frac{\pi}{2F}\right] = j_L(\alpha)\cos\frac{\pi}{2F}\cos\left(\phi - \frac{\Delta}{2}\right) + \frac{\sin\Delta}{2} \quad (31)$$

Equating (24), (28), using the expressions derived in (26) for $m_C(0)$ and (25) for $j_L(0)$ in (24), the following relationship can be arrived at by rearranging the terms and using basic algebra

$$\cos\Delta[\cos\alpha + (j_L(\alpha) + J)\sin\alpha - 1] - \sin\Delta[\sin\alpha - (j_L(\alpha) + J)\cos\alpha] = 1 - \cos\beta + [j_L(\alpha) - J]\sin\beta \quad (32)$$

Before solving the expression above by expanding and using trigonometric identities, the following definition is made for the sake of brevity in expressions

$$K = \left[\cos\frac{\pi}{2F} + J\sin\frac{\pi}{2F}\right] \quad (33)$$

Expanding (32) and using basic trigonometric identities, the following relationship can be arrived at

$$K\cos\left(\phi - \frac{\Delta}{2}\right) = j_L(\alpha)\cos\frac{\pi}{2F}\sin\left(\phi - \frac{\Delta}{2}\right) + \frac{1+\cos\Delta}{2} \quad (34)$$

Substituting (33) in (31), we can arrive at the following expression for $j(\alpha)$ in terms of the other parameters.

$$j_L(\alpha) = \frac{-\frac{\sin\Delta}{2} - K\sin\left(\phi - \frac{\Delta}{2}\right)}{\cos\frac{\pi}{2F}\cos\left(\phi - \frac{\Delta}{2}\right)} \tag{35}$$

Substituting the expression derived for $j_L(\alpha)$ from (35) in (34) we can arrive at the following intermediate expression

$$K\cos\left(\phi - \frac{\Delta}{2}\right) = \frac{-\frac{\sin\Delta}{2} - K\sin\left(\phi - \frac{\Delta}{2}\right)}{\cos\left(\phi - \frac{\Delta}{2}\right)}\sin\left(\phi - \frac{\Delta}{2}\right) + \frac{1+\cos\Delta}{2} \tag{36}$$

Relationship in (36) shall be further reduced using basic trigonometric identities to arrive at the final expression for ϕ in terms of the control parameters, normalized switching frequency F, load current J and PWM period Δ as given below

$$\phi = \pm\cos^{-1}\left[\frac{1}{\cos\frac{\Delta}{2}}\left(\cos\frac{\pi}{2F} + J\sin\frac{\pi}{2F}\right)\right] \tag{37}$$

The gain of the converter in PWM mode of operation can now be given by the expression below

$$M = \frac{2F}{\pi}\left[\phi + j_L(\alpha)\right] \tag{38}$$

where, ϕ is defined in (37) and $j_L(\alpha)$ is defined in (35). This is the final expression for the gain of the converter in the PWM mode of operation. The gain of the converter in the VFM mode is a special case of this expression which can be arrived at by substituting $\Delta = 0$ in (35) and (37). The expression for the gain in the VFM is now derived as given below

$$M = \frac{2F}{\pi}\left[\phi - \frac{\sin\phi}{\cos\frac{\pi}{2F}}\right] \tag{39}$$

The expression of the converter gain in (39) matches with the derived expression in [16]. Based on the closed form expression derived for the gain of the converter, the expressions for other parameters of interest can now be derived.

$$\alpha = \frac{\gamma - \Delta}{2} - \phi \tag{40}$$

$$\beta = \frac{\gamma - \Delta}{2} + \phi \tag{41}$$

$$j_L(0) = J - \cos\alpha\left[j_L(\alpha) + J\right] + \sin\alpha \tag{42}$$

$$m_C(0) = \cos\alpha + \sin\alpha\left[j_L(\alpha) + J\right] - 1 \tag{43}$$

$$j_L(\beta) = J + \cos\beta\left[j_L(\alpha) - J\right] + \sin\beta \tag{44}$$

$$m_C(\beta) = m_C(0)\cos\Delta - \sin\Delta\left[j_L(0) - J\right] \tag{45}$$

IV. Experimental Results

The modulation strategy is verified in LTSpice simulation and validated with an experimental prototype as shown in Fig. 7. The details of the resonant tank and load conditions are given in Table III. The DC bus voltage is $V_{dc} = V_b = 390V$. Based on the resonant tank components in Table III, resonant or base frequency, $f_b = 61.7kHz$. The required PWM signals for the HF DC-AC converter is generated from a controller based on the TMS320F2808 μController. An effective dead time of $750ns$ is provided between the switching of devices on the same leg.

The converter shall be operated at $86kHz$ which corresponds to $F = 1.4$. The duty ratio chosen for operation is $\Delta = 0.466$. From (7), (37) and (36), converter gain, M is expressed as a function of F, J and Δ and given by $M = G(F, J, \Delta)$. PU Load resistance, $Q = R/R_b$ and from the value of R given in Table III, $Q = 0.766$. Q is also given as $\frac{M}{J}$. From these two relationships, we can recursively solve $M = G(F, \frac{M}{Q}, \Delta)$ to find M. The resultant value of $M = 0.418$ which corresponds to an output voltage of $111.2V$.

TABLE III
Prototype Component Details

Description	Value
Active Switches	IRGP50B60PD
Diodes	IDW30S120
Resonant Inductor	73.8μH 31 Turns, Ferrite Core - EE80-38-20
Transformer	Turns ratio ($N_1 : N_2$) - 20:14
Resonant Capacitor	194.7nF, WIMA FKP1 series, 2X4 bank of 100 nF
Load Resistance	10.91Ω

The converter is simulated using LTSpice and operated in the Experimental test setup as shown in Fig. 8(a). Fig. 8(a) and Fig. 8(b) shows the key waveforms in simulation and experiment respectively. It can be observed that there's good concurrence between these waveforms. Table IV provides a

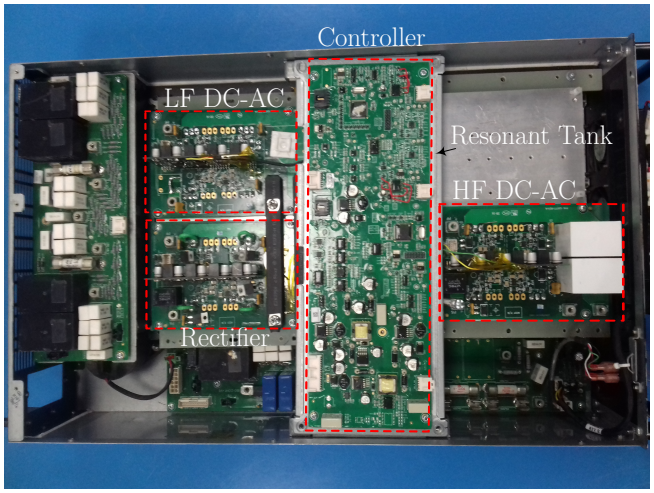

Fig. 7. Hardware Prototype

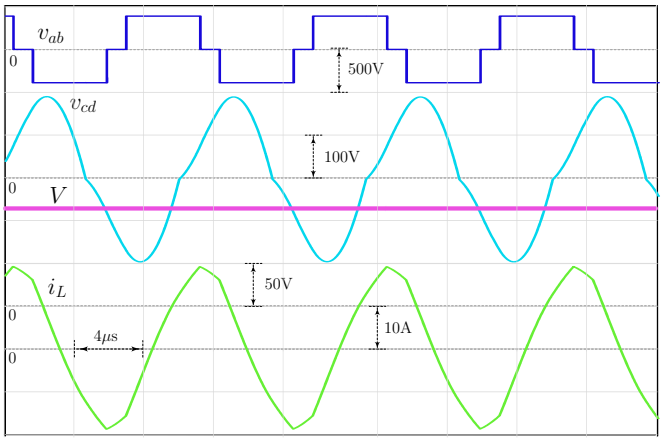

(a) Simulation - Tank Voltage, v_{ab},Cap voltage, v_{cd}, Output Voltage, V,Inductor Current, i_L

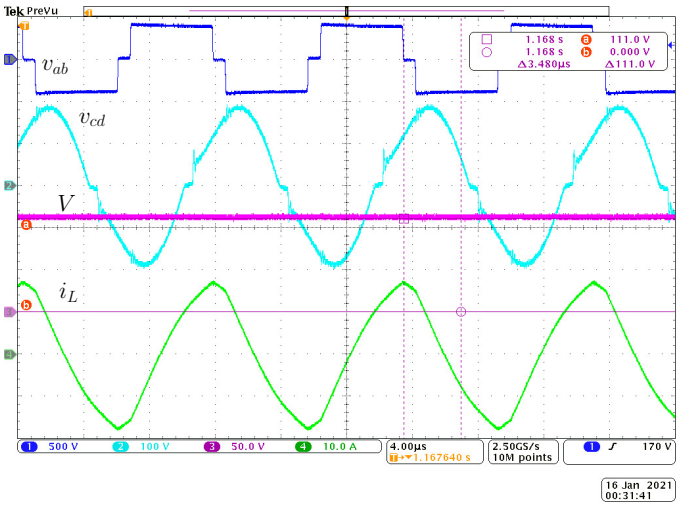

(b) Experiment - [CH1]-500 V/div, [CH2]-100 V/div, [CH3]-50 V/div, [CH4]-10 A/div

Fig. 8. Experimental and Simulation Results - (a) Simulation Results (b) Experimental waveforms

quantitative comparison of the results obtained through analysis, simulation and experiment. From the observed data in this table, the presented analysis is validated through simulation and experiment.

TABLE IV
COMPARISON BETWEEN ANALYSIS, SIMULATION AND EXPERIMENT

Parameter	Analysis	Simulation	Experiment
Output, MV_b (V)	111.2	112.2	111.0
$j_L(\alpha)I_b$ (A)	12.07	12.55	12.00
$j_L(0)I_b$ (A)	15.66	15.89	15.00
$m_C(0)V_b$ (V)	163.0	166.4	170.0
$j_L(\beta)I_b$ (A)	18.65	18.98	17.40

V. CONCLUSION

The exact state-plane based analysis of the parallel resonant converter is presented for fixed frequency phase-shift modulation. The fixed frequency phase-shift modulation has advantages like simpler magnetics and controller design and avoids complexity of switching signal generation in variable frequency-based modulation techniques. But the existing fundamental harmonic approximation-based analysis results in estimation error. The presented exact analysis gives the closed form expression of the converter gain as a function of zero period, frequency, and load current. The expressions of key intermediate parameters are also presented. The theoretical analysis is experimentally validated with a $1.5kW$ hardware prototype and in Simulation. The presented closed-form expressions will help to optimally design PRC with phase-sift modulation.

REFERENCES

[1] M. T. Outeiro, G. Buja, and D. Czarkowski, "Resonant power converters: An overview with multiple elements in the resonant tank network," *IEEE Industrial Electronics Magazine*, vol. 10, no. 2, pp. 21–45, June 2016.

[2] D. V. S. Kouro, J. I. Leon and L. G. Franquelo, "Grid-connected photovoltaic systems: An overview of recent research and emerging pv converter technology," *IEEE Industrial Electronics Magazine*, vol. 9, no. 1, pp. 47–61, March 2015.

[3] K. Park, C. Kim, G. Moon, and M. Youn, "Voltage oscillation reduction technique for phase-shift full-bridge converter," *IEEE Transactions on Industrial Electronics*, vol. 54, no. 5, pp. 2779–2790, Oct 2007.

[4] S. Tian, F. C. Lee, and Q. Li, "A simplified equivalent circuit model of series resonant converter," *IEEE Transactions on Power Electronics*, vol. 31, no. 5, pp. 3922–3931, 2016.

[5] H. Vu and W. Choi, "A novel dual full-bridge llc resonant converter for cc and cv charges of batteries for electric vehicles," *IEEE Transactions on Industrial Electronics*, vol. 65, no. 3, pp. 2212–2225, 2018.

[6] A. K. Rathore, D. R. Patil, and D. Srinivasan, "Non-isolated bidirectional soft-switching current-fed lcl resonant dc/dc converter to interface energy storage in dc microgrid," *IEEE Transactions on Industry Applications*, vol. 52, no. 2, pp. 1711–1722, 2016.

[7] C. Yeh, C. Chen, M. Lee, and J. Lai, "A hybrid modulation method for single-stage soft-switching inverter based on series resonant converter," *IEEE Transactions on Power Electronics*, vol. 35, no. 6, pp. 5785–5796, 2020.

[8] D. G. Bandeira, T. B. Lazzarin, and I. Barbi, "High voltage power supply using a t-type parallel resonant dc dc converter," *IEEE Transactions on Industry Applications*, vol. 54, no. 3, pp. 2459–2470, 2018.

[9] Y. Chen, J. Xu, Y. Wang, L. Lin, and J. Cao, "A dual-carrier modulation technique for half-bridge resonant converter with wide soft-switching range," *IEEE Transactions on Industrial Electronics*, vol. 66, no. 1, pp. 223–232, 2019.

[10] N. Harischandrappa and A. K. S. Bhat, "A fixed-frequency zvs integrated boost dual three-phase bridge dc dc lcl-type series resonant converter," *IEEE Transactions on Power Electronics*, vol. 33, no. 2, pp. 1007–1023, 2018.

[11] A. Trigui, S. Hached, F. Mounaim, A. C. Ammari, and M. Sawan, "Inductive power transfer system with self-calibrated primary resonant frequency," *IEEE Transactions on Power Electronics*, vol. 30, no. 11, pp. 6078–6087, 2015.

[12] A. K. Paul, "Robust features of sosmc guides in quality characterization of tank circuit in air-cooled induction cap sealing," *IEEE Transactions on Industry Applications*, vol. 54, no. 1, pp. 755–763, 2018.

[13] U. Kundu and P. Sensarma, "A unified approach for automatic resonant frequency tracking in llc dc dc converter," *IEEE Transactions on Industrial Electronics*, vol. 64, no. 12, pp. 9311–9321, 2017.

[14] R. L. Steigerwald, "A comparison of half-bridge resonant converter topologies," *IEEE Transactions on Power Electronics*, vol. 3, no. 2, pp. 174–182, April 1988.

[15] Y. Chen, J. Xu, J. Sha, L. Lin, and J. Cao, "An improved fundamental harmonic approximation to describe filter inductor influence on steady-state performance of parallel-type resonant converter," *IEEE Transactions on Power Electronics*, vol. 34, no. 3, pp. 2467–2478, March 2019.

[16] S. D. Johnson and R. W. Erickson, "Steady-state analysis and design of the parallel resonant converter," *IEEE Transactions on Power Electronics*, vol. 3, no. 1, pp. 93–104, Jan 1988.

[17] A. Kumar, A. Awasthi, O. Salari, S. Bagawade, and P. Jain, "A novel time domain analysis of the llc-l resonant converter for the use of the cll and llc resonant converter," in *2019 IEEE Applied Power Electronics Conference and Exposition (APEC)*, 2019, pp. 3453–3460.
[18] S. D. Johnson, "Steady state analysis and design of the parallel resonant converter," 1984.